# Simulation of Cooling and Pressure Effects on Inflated Pahoehoe Lava Flows

Lori S. Glaze[1] and Stephen M. Baloga[2]

[1]NASA GSFC

Lori.S.Glaze@nasa.gov

[2]Proxemy Research

sbaloga1@starpower.net

Accepted for publication in JGR

18 November 2015

**Abstract:**

Pahoehoe lobes are often emplaced by the advance of discrete toes accompanied by inflation of the lobe surface. Many random effects complicate modeling lobe emplacement, such as the location and orientation of toe breakouts, their dimensions, mechanical strength of the crust, micro-topography and a host of other factors. Models that treat the movement of lava parcels as a random walk have explained some of the overall features of emplacement. However, cooling of the surface and internal pressurization of the fluid interior has not been modeled. This work reports lobe simulations that explicitly incorporate 1) cooling of surface lava parcels, 2) the propensity of breakouts to occur at warmer margins that are mechanically weaker than cooler ones, and 3) the influence of internal pressurization associated with inflation. The surface temperature is interpreted as a surrogate for the mechanic strength of the crust at each location and is used to determine the probability of a lava parcel transfer from that location. When only surface temperature is considered, the morphology and dimensions of simulated lobes are indistinguishable from equiprobable simulations. However, inflation within a lobe transmits pressure to all connected fluid locations with the warmer margins being most susceptible to breakouts and expansion. Simulations accounting for internal pressurization feature morphologies and dimensions that are dramatically different from the equiprobable and temperature-dependent models. Even on flat subsurfaces the pressure-dependent model produces elongate lobes with distinct directionality. Observables such as topographic profiles, aspect ratios, and maximum extents should be readily distinguishable in the field.

## 1. Introduction.

Numerous models with various degrees of complexity treat terrestrial and planetary lava flows as gravity-driven viscous or turbulent fluids on an inclined plane [e.g., *Nichols*, 1939; *Shaw and Swanson*, 1970; *Danes*, 1972; *Harrison and Rooth*, 1976; *Baloga*, 1987; *Baloga et al*., 1995; *Baloga et al.,* 1998; *Harris and Rowland*, 2001; *Baloga et al*., 2001; *Rowland et al*., 2004; *Baloga and Glaze*, 2008; *Glaze et al.*, 2009; *Glaze et al*., 2014]. These models consider the influence of large-scale forces like gravity, pressure, and momentum, on the bulk flow and are usually intended to estimate the emplacement parameters from the dimensions, morphology and pre-existing slope of the flows. Such parameters include volumetric flow rate, duration of lava supply, flow advance rate, and rheologic characterizations of Newtonian or Bingham fluids. Although the rubbly channelized a`a flow shown in a 1a exhibits elements of randomness, the overall dynamics of the flow are governed by the systematic force of gravity and volume conservation between the active flow and the embanking levees [e.g., *Baloga et al*, 1998*; Glaze et al.,* 2009]. As a result, the list of models above use a deterministic approach that is appropriate for a`a flows such as that shown in Figure 1a. For a given boundary or initial condition, a deterministic model always produces the identical outcome. In the case of a lava flow, once the flow rate, rheology and slope are specified, a deterministic model will always produce exactly the same advance rate and flow depth as a function of time or distance.

The recognition of inflation in pahoehoe lava flows by *Hon et al.* [1994] revolutionized thinking about the style, pervasiveness, and importance of pahoehoe emplacement on the Earth, Mars, and Io [*Self et al.*, 1996, 1998; *Thordarson and Self,* 1998; *Keszthelyi et al.,* 1999, 2000, 2006]. In contrast to the a`a flow shown in Figure 1a, the pahoehoe deposit in Figure 1b is dominated by randomness in size, shape and orientation of individual volume elements (referred

44 to here as toes). This mode of flow emplacement is characterized by toe formation and inflation
45 [e.g., *Rowland and Walker,* 1990*; Hon et al.,* 1994 *Keszthelyi et al.,* 1999*; Baloga and Glaze,*
46 *2003; Harris et al., 2007; Keszthelyi et al.,* 2006; *Hamilton et al*., 2013]. High-resolution images
47 of lava flows on Mars indicate that both channelized a`a and pahoehoe styles of emplacement
48 may also occur in planetary environments (Figure 2). In the pahoehoe toe regime, stagnation,
49 inflation, and toe formation are most closely tied to the final topography, dimensions, and
50 morphologic features. The combination of low slopes and low flow rates typical of pahoehoe
51 emplacement results in minimal disruption of a rapidly forming, insulating crust [*Hon et al.,*
52 1994]. The efficient crustal insulation limits cooling to conduction only, allowing the interior
53 lava to remain fluid for long periods of time in contrast to a`a flows where fresh lava is
54 continuously exposed at the surface [e.g., *Crisp and Baloga*, 1990; *Wright and Flynn*, 2003,
55 *Wright et al*., 2011].

56 Although the forces of gravity, pressure and momentum are present in pahoehoe
57 emplacement, other influences act on each individual volume element, or parcel, of lava with a
58 randomizing effect. The mechanical strength of the cooling surface, pressure, crystallization,
59 micro-topography (i.e., centimeter-scale relief) and similar factors cause non-gravitational forces
60 to dominate the dynamics of emplacement. These forces at the parcel-scale are subject to natural
61 variations that necessitate an approach, different from the classical deterministic models, that
62 accounts for ubiquitous random effects and inflation.

63 In current practice, models of a`a flows are generally set up by considering the forces that act
64 on control volumes that slice through the flow from the underlying surface to a height
65 characteristic of the entire flow depth. In theory, one could divide a large lava flow up into tiny
66 volume parcels and consider the effects of these forces on each volume element. However, for

large flows (e.g., channelized a`a flows), such an approach significantly increases computational complexity without adding significant new information. The essential effects of fluid flow are retained when one considers a volume element that is equal to the full thickness and width of the flow (a control volume up to many tens of cubic meters).

For pahoehoe flows that are dominated by random effects, the scale has been set in recent works at a parcel scale typical of an individual toe [*Glaze and Baloga*, 2013], with a volume of $0.75 \times 0.66 \times 0.2$ m$^3$ [Crown and Baloga, 1999]. At this scale, a parcel at the surface of a lobe is subject to many forces with random effects. These include forces associated with cooling, cracking, rupturing, stretching and various forces from neighboring parcels on the surface and beneath the parcel. A parcel in the interior of a lobe may be influenced by forces associated with internal processes such as crystallization and vesiculation, and external forces from neighboring parcels with a different rheology, momentum, shear state, crystal content and ultimately the propagated influence of the underlying lobe topography and the mechanical strength of the crust and visco-elastic layers. Thus, for a pahoehoe lobe, the behavior of the individual parcels (at the scale of a typical toe) must be considered and then aggregated together to understand the overall properties of the entire lobe.

The fundamental difficulty in developing a new model for pahoehoe lava flows is that the random effects associated with inflation, internal fluid pressure, and crustal strength dominate the emplacement [*Hon et al*. 1994*; Thordarson and Self,* 1998*; Keszthelyi et al.,* 1999*; Crown and Baloga, 1999; Baloga and Glaze, 2003; Harris et al., 2007; Glaze and Baloga, 2013]*. Thus, in contrast to a deterministic approach, a model that includes random effects produces a distribution of outcomes for the same given boundary or initial conditions. In the case of a lava flow with the same specification of flow rate, rheology and slope as a deterministic model, each

90 run (or simulation) of a random model will result in a slightly different advance rate and flow
91 depth as a function of time or distance.

92 When many runs of a random model are performed, the suite of advance rates and flow depths
93 results in a distribution of these variables with some mean values and dispersions. Assuming the
94 basic physics is the same for these two types of approaches, one would presume that the mean
95 values of the random model approach those of the deterministic model if enough random
96 simulations are performed.

97 The key point is that there is uncertainty associated with the outcomes of a random model.
98 With only one run, there is no way to determine whether a particular simulation has produced an
99 outcome near the mean value or something that is rather unlikely. This can only be determined
100 by acquiring enough simulations to gauge the dispersion of the outcomes.

101 *Baloga and Glaze* [2003] developed an initial 2-dimensional model for pahoehoe
102 emplacement based on classical uncorrelated and correlated random walks [C*handrasekar*,
103 1943]. They showed that a wide variety of field observables could be explained by such an
104 approach. The topographic profiles of simple lobes, the tendency for central channel
105 development, frontal steepening and similar pahoehoe manifestations were broadly in agreement
106 with field observations. However, the computational requirements for further advances at that
107 time were intractable.

108 *Glaze and Baloga* [2013] presented a more comprehensive model that simulated random
109 transfers of individual lava parcels within a pahoehoe lobe as a function of space and time. The
110 model was based on volume conservation and a set of probability rules for the parcel transfers.
111 The output of the model (Figure 3) was 3-dimensional topography that showed how the lobe
112 thickened and expanded with time subject to a variety of factors such as the source geometry,

113 confining barriers, and volumetric flow rate. Of particular interest was the degree of lobe
114 inflation, i.e., the degree to which the existing lobe thickens at the expense of expansion at the
115 margins. The basic model described in *Glaze and Baloga* [2013] assumes that all occupied basal
116 locations are equally likely to be the site of the next parcel transfer and is referred to here as the
117 'equiprobable' model.

118 The statistical concept of correlation [*Sheskin*, 1997] in lava transfers (i.e., the statistical
119 dependence of one lava parcel movement on another) was also explored by *Glaze and Baloga*
120 [2013]. Correlation in the lava transfers at the margin was shown to have a significant effect on
121 the lateral expansion, the thickness profiles and the rate of expansion of the lobe. However,
122 plausible physical causes for the correlation were addressed only in general terms.

123 The most obvious physical process omitted from the earlier models was the cooling of the
124 outer surface of the lobe. The primary issue is the extent to which such cooling would influence
125 the morphology, dimensions and inflation of the lobe. Another physical process omitted from
126 the earlier models is the role of the internal fluid pressure. The simulations of *Glaze and Baloga*
127 [2013] clearly showed local topographic highs and lows within the lobe that would pressurize all
128 connected parts of the hot mobile fluid interior. Thus one might expect topographic gradients to
129 influence breakouts in remote parts of the lobe as is often observed in the field.

130 In this work the explicit cooling of surface parcels has been added to the simulation approach
131 Glaze *and Baloga* [2013]. The temperature of the surface units is modeled by Hon's surface
132 cooling formula [*Hon et al*., 1994]. The probability rules of *Glaze and Baloga* [2013] have been
133 modified to increase the probability of a transfer when the surface temperature is relatively high
134 and decrease transfer probabilities for cooler parcels. Simulations of this process are referred to
135 as the 'temperature-dependent' model.

136 Another modification of the probability rules of *Glaze and Baloga* [2013] addresses the
137 influence of inflation within the lobe, resulting in a third distinct type of simulation. Inflation is
138 defined here as an increase in lobe volume with no concurrent increase in lobe area. Internal
139 transfers within an existing lobe result in a local inflation that produces topographic high points.
140 Basic physics considerations suggest that the increase in lobe thickness causes an increase in the
141 pressure throughout all connected parts of the fluid interior, whether near the topographic high or
142 not. Such an increase in pressure increases the probability of a breakout at the mechanically
143 weaker confining locations of the lobe. The third type of simulation in this work forces breakouts
144 to occur at the weaker locations of the lobe as governed by the cooling of the surface units.
145 Simulations of this process are referred to as the 'pressure-dominated' model. Opportunities for
146 future theoretical and field studies are given in conclusion.
147
148 **2. The Simulations**
149 The term 'simulation' in this work means specifically that one or more of the input quantities
150 of the simulation is a random variable. In a simulation, a particular value of each random
151 variable is drawn from a prescribed probability distribution. Each simulation represents a single
152 trial or 'realization' of all the output observables at the end of the simulation. Due to
153 randomness, each simulation produces a different set of outcomes depending on the nature of the
154 underlying probability distributions. Use of this simulation approach allows exploration of the
155 range of expected outcomes for each case of prescribed probabilities.
156 Each of the three simulation cases examined here ('equiprobable', 'temperature-dependent',
157 and 'pressure-dominated') is based on different sets of probabilistic rules for lava transfers that
158 are based on different physical considerations. All simulations assume a flat pre-existing surface,

159 with a constant rate of lava supply, where each parcel volume of 0.09 $m^3$ is equal to a typical
160 pahoehoe toe (see *Glaze and Baloga* [2013] for more details on the basic model). Because the
161 volume of a lava parcel is fixed, the volumetric supply rate can be adjusted by simply changing
162 the time interval between parcel additions at the source. A time interval of 15 seconds is used in
163 the results presented below, based on average volume supply rates observed for a small (< 10.4
164 $m^3$) toe lobe in Hawaii [*Hamilton et al*., 2013]. Time varying and fluctuating supply rates can be
165 modeled by modulating the time interval between parcel additions at the source. Such analyses
166 are reserved for future analyses.
167
168 **2.1. Equiprobable Simulations.**
169 In the equiprobable case, the probability of a transfer of lava at each time step of the
170 simulation is considered to be a constant for all basal locations within a lobe that are occupied by
171 at least one lava parcel [*Glaze and Baloga*, 2013]. There are two random selections by the
172 algorithm at each time step. The first determines the basal cell location that will be the source of
173 the next transfer. The second determines the direction of the next transfer from the source
174 location (i.e., north, south, east or west). The dimensions and morphology of the lobe are
175 updated with each time step. A comprehensive description of this type of simulation is given in
176 *Glaze and Baloga* [2013].
177 The simulated equiprobable lobe shown in Figure 3 assumes a single parcel as the lobe
178 source, and subsequent release of 2500 additional lava parcels. Using 0.09 $m^3$ as the typical
179 volume of an individual toe [*Crown and Baloga*, 1999], the total volume of the lobe is 225 $m^3$.
180 This is consistent with the range of volumes reported in field studies of lobes emplaced

181 predominantly in the toe regime [*Crown and Baloga,* 1999; *Baloga and Glaze*, 2003; *Hamilton*
182 *et al.,* 2013].
183
184 **2.2. Temperature-Dependent Simulations.**
185 Ultimately, the mechanical strength of the crust controls the movement of lava within the lobe
186 and at its margins. The surface temperature is taken here as a proxy for the mechanical strength
187 of the crust. The surface cooling rates of pahoehoe lavas are well known, both from theoretical
188 and empirical studies [e.g., *Harris and Baloga*, 2009; *Crisp and Baloga*, 1990; *Hon et al.*, 1994;
189 *Wright and Flynn*, 2003]. The fundamental assumption of the temperature-dependent approach
190 is that warmer parcels are more likely to be the site of the next transfer than cooler ones.
191 Specifically, it is assumed that the probability of a lava parcel transfer at a particular location is
192 directly proportional to the temperature of the surface parcel at that location. Mathematically, the
193 probability that basal location $j$ at time $t$ is the site of the next parcel transfer is

194 $$P_j(t) = \frac{T_j(t)}{\sum_i T_i(t)} \qquad (1)$$

195 where $T_j(t)$ is the temperature of the surface at location $j$ and the $i$ summation is taken over all
196 occupied basal locations at time $t$. Once the location for the lava transfer has been determined by
197 (1), the current algorithm treats the four possible directions for the lava transfer as equiprobable.
198 The simulations assume that a parcel of lava begins to cool when a cell is first occupied and
199 thus exposed to the atmosphere. Other parcels may be transferred to that cell location, but are
200 assumed to increase the volume (inflate) at that location, keeping the original cell on the surface
201 to continue cooling. The empirical formula of *Hon et al*. [1994] is used to cool each surface
202 parcel separately for each time step of the lobe emplacement.

$$T(t) = -60.8\ln(t) + 303 \quad (2)$$

where $t$ is measured in hours and $T$ is given in $^{o}$C.

In the present model, internal transfers only inflate the lobe locally and leave the pre-existing crust undisturbed and continuing to cool. Heat is propagated through the crust very slowly [e.g., *Crisp and Baloga*, 1990; *Harris and Rowland*, 2001]. Thus, it is assumed that only the surface parcels (20 cm thick) cool to any significant degree. For the emplacement times considered here (1/2 – 5 hours) the thermal boundary layer penetrates only to a few cm or less (*Hon et al*., 1994, e.g., Figure 10; *Crisp and Baloga*, 1990)

The thermal properties of basaltic crust that insulate the fluid interior have been documented for many years (e.g., *Peck*, 1978; *Crisp and Baloga*, 1990; *Lipman and Banks*, 1987; *Moore,* 1987; *Hon et al.*, 1994). Thus in this work the interior parcels are assumed to remain at a constant temperature (~1140 ºC [*Lipman and Banks*, 1987]) until they break out into an unoccupied cell at the existing margin of the lobe. The initial surface temperature of a breakout at the margin (occupation of a new cell location) is set to 1140 ºC no matter when it occurs in the simulation. Subsequently the breakout parcel cools according to the formula of *Hon et al.* [1994].

Figure 4 shows the *Hon et al.* [1994] cooling curve for a time period of 24 minutes. For a lobe with sixteen parcels, and 1.5 minute time steps (equivalent to an extremely low volume flow rate used here for illustrative purposes only), the surface temperatures are indicated by the arrows, where Parcel 1 (transferred at Time $t_1$) is the coolest, and Parcel 16 is the warmest.

In the temperature-dependent model, the probability for a parcel transfer is weighted by the surface temperature. The probability distribution for determining which location will be selected for the next parcel transfer is obtained by summing the temperatures of all surface parcels to obtain a normalization at that particular time step. The assigned probability for a transfer at a

226 given location is simply the current surface temperature at that location divided by the
227 normalization at that time step. The example in Figure 5 illustrates the companion, normalized
228 probability (density) for the example in Figure 4, where the equiprobable case is also shown for
229 comparison.

230 Two typical 200-parcel examples of the temperature-dependent simulation are shown in
231 Figure 6. In these simulations, a parcel of lava volume was added to the lobe every 15 seconds,
232 such that the lobe was emplaced in 50 minutes. Although there is a great deal of variability and a
233 number of complicating factors (e.g., changes in topography, lava supply rate), such an
234 emplacement time is reasonably consistent with a lobe volume of 18 $m^3$ (200 parcels $\times$ 0.09$m^3$).

235 The general topography and morphology of these lobes is very similar to the equiprobable
236 case. The physical basis for this is that the cooling of the surface parcels is so rapid that most
237 parcels are on the long flat end of the cooling curve (Figure 4) and thus have roughly the same
238 probability of a transfer. There is a slight difference however, as suggested by the elevated
239 surface temperatures at the margin.

240 A measurable quantity of interest is the maximum extent of the lobe from the source. This
241 distance is denoted as $r_{max}$. To compare the temperature-dependent and equiprobable cases, 300
242 simulations were done for each approach. For each individual simulation the maximum distance
243 from the source was computed for a lobe of 200 parcels. The results are shown in Figure 7a. The
244 shape of the distribution of $r_{\max}$ in both cases is very similar to a lognormal distribution. The
245 temperature-dependent simulations have a slightly higher mean value, meaning that the
246 temperature-dependent cases tended to travel somewhat farther than the equiprobable cases.

247 Given the great degree of variability (i.e., the high standard deviations) of both simulation
248 approaches it is highly unlikely that these two emplacement scenarios could be distinguished in

249 the field. Moreover, there are a host of other complicating factors, such as variations in pre-
250 existing topography, lava supply and so forth that would complicate the discrimination.
251
252 **2.3. Pressure-Dominated Simulations.**
253 These simulations extend the temperature-dependent algorithm by including the influence of
254 internal fluid pressure increases due to inflation. When there is an internal lava transfer to a
255 location within the lobe the thickness at that location increases. This local inflation increases the
256 fluid pressure not only at that location, but also at all connected fluid locations within the lobe.
257 This is similar to inflating a balloon with various mechanical strengths at different parts of its
258 surface.
259 The pressure-dominated algorithm captures the influence above by using a combination of
260 random and systematic influences on the parcel transfers. When there are no internal transfers
261 (and thus no inflation), the location of the next breakout is determined randomly from the
262 probabilities derived from the local surface temperatures, i.e., fresh locations have a higher
263 probability than older ones (identical to the temperature-dependent case). However, the rules
264 change somewhat after there have been internal transfers (Figure 8). After one or more internal
265 transfers, there will eventually be a 'breakout' where a parcel will be transferred to a previously
266 unoccupied cell. When this happens, the pressure-dominated model assumes that the build up of
267 pressure results in the systematic selection of the last breakout location as the source in the next
268 time step and only the direction of the subsequent breakout is chosen at random.
269 The inclusion of inflation pressure in this way has a dramatic effect on the morphology and
270 dimensions of the lobe particularly its plan form shape and maximum length (Figure 9). The
271 pressure influence in the algorithm provides a statistical correlation, i.e., a systematic effect

imposed on the randomness. Such correlations were suggested in *Baloga and Glaze* [2003] and *Glaze and Baloga* [2013], but were only vaguely attributed to possible physical causes. Here the correlations in lava transfers are specifically attributed to an increase in the hydrostatic pressure within the lobe and a temperature-dependent weakness at the margin.

The pressure-dominated simulations have a distinct lobate morphology that is markedly different from the more axisymmetric equiprobable and temperature-dependent simulations. The examples in Figure 9 show the concentration of warmer parcels toward the front of the advancing lobes. In particular, it is interesting to compare Trial 2 to the equiprobable and temperature-dependent cases. Despite the extent of the flow being similar to the equiprobable and temperature-dependent simulations, the surface temperature distribution is quite different from those in Figure 6. The pressure-dominated simulations show a very marked directionality with the warmer parcels clustered at the end of the lobe, even though the flow has wrapped around on itself, whereas the temperature-dependent lobes have warm parcels distributed along the entire margin of the lobe.

The distribution of maximum distances from the source is shown in Figure 7b for 300 simulations of 200 parcels each at 15 second intervals. The mean value of $r_{max}$ is now 13.2 parcels, almost double the equiprobable and temperature-dependent cases. Because the total volume of all the simulations has been held fixed, the greater length of these lobes gives a much thinner overall thickness as noted in *Glaze and Baloga* (2013).

Despite the more lobate plan form and relatively smaller thicknesses, the pressure-dominated lobes exhibit comparable degrees of inflation, retaining this ubiquitous pahoehoe emplacement characteristic. Figure 10 shows the rate of inflation for a typical equiprobable reference case versus two typical examples of the pressure-dominated case, all with 200 parcel simulations. It is

295 readily seen that the overall vertical growth the lobe is essentially the same. Unlike the
296 morphology and extent of the lobe, this aspect of emplacement cannot be used to distinguish the
297 underlying physical processes.
298
299 **3. Conclusions.**
300 This work shows that the cooling of the surface alone has little influence on the morphology,
301 dimensions and the rates of lateral expansion and inflation compared to the equiprobable,
302 temperature-independent simulations of *Glaze and Baloga* [2013]. Lobes with surface parcels
303 that cool according to Hon's formula [*Hon et al.*, 1994] retain the approximate Gaussian
304 topography and symmetric plan form identified by field observations and the earlier temperature-
305 independent simulations [*Crown and Baloga*, 1999; *Baloga and Glaze* 2003; *Glaze and Baloga*,
306 2013]. The differences in morphology, dimensions, aspect ratios, and maximum extents from the
307 source for lobes with cooling and constant temperature surface units are so slight they are
308 unlikely to be distinguishable in the field. Such a result might be anticipated intuitively for this
309 emplacement regime (e.g., 200 parcels released at 15 second intervals) because radiative cooling
310 is so rapid that most locations within the lobe have approximately the same probability for an
311 internal lava transfer or breakout at the margin.
312 When the internal inflation pressure originally identified by *Hon et al.* [1994] causes
313 systematic breakouts at the warmest (and therefore weakest) margins, the morphologies and
314 dimensions of the simulated lobes are dramatically different from the purely temperature-
315 dependent and equiprobable cases. The internal fluid pressure due to inflation is felt uniformly
316 with all contiguous fluid regions within a lobe so that the warmest and weakest margins become
317 the most likely locations for margin expansion. This is a physical explanation for the correlations

318 considered in *Baloga and Glaze* [2003] and *Glaze and Baloga*, [2013]. Both works concluded
319 that correlation was required to explain a variety of observed lobe features such as directionality,
320 aspect ratio, topographic cross-lobe profiles and the tendency to form channels and embanking
321 levees.

322 It is the combination of inflation pressure and the mechanical weakness of the warmer and
323 weaker margins that causes lobes to become significantly more elongate than their temperature-
324 dependent and equiprobable counterparts. The overall thickness and plan form shapes of lobes
325 formed by this process are readily distinguishable from the temperature-dependent and
326 equiprobable cases. The evolving surface temperature distributions of the pressure-dependent
327 lobes are also readily distinguishable from the purely temperature-dependent and equiprobable
328 cases. It is noteworthy, however, that the time-dependent rate of inflation remains essentially the
329 same in all cases.

330 The types of simulations performed in this work offer the promise of developing quantitative
331 inferences about emplacement conditions from the dimensions and morphologies of pahoehoe
332 lobes that were not observed while they were active. Comprehensive field campaigns for active
333 lobes with a range of local discharge rates are needed to identify the appropriate model for
334 detailed data-theory comparisons. These measurements should include pre-existing topography,
335 time-series changes in flow morphology, and thermal imaging. This would permit isolation of
336 the different physical processes governing the shape and dimensions of the lobe and a statistical
337 characterization of the random effects. The next steps in advancing these models are the
338 incorporation of an underlying regional slope and the influence of micro-topography. Such
339 advances would provide a methodology for developing quantitative inferences about the
340 unobserved emplacement of terrestrial and planetary pahoehoe lava flows.

## 4. Acknowledgements.

The authors would like to thank S. Rowland, D. Crown, and A. Harris, S. Self, T. Thordarson and C. Hamilton for numerous detailed discussions of pahoehoe emplacement observations. This work was conducted under NASA Planetary Geology and Geophysics grants WBS 811073.02.01.05.80 and WBS 8110073.02.01.06.60 for LSG, and NNX13AR12G for SMB. Simulation results used to generate figures in this paper are available upon request.

349 **REFERENCES**


350 Baloga, S.M., Lava flows as kinematic waves, J Geophys Res, 92(B9), 9271-9279, 1987.

351 Baloga, S., and L.S. Glaze, Pahoehoe transport as a correlated random walk, J Geophys Res, 108
352 (B1), 2031, doi:10.1029/2001JB001739, 2003.

353 Baloga, S., and L.S. Glaze, Self-replication model for long channelized lava flows on the Mars
354 plains, J Geophys Res, 113, E05003, doi:10.1029/2007JE002954, 2008.

355 Baloga, S.M., P.D. Spudis, and J.E. Guest, The dynamics of rapidly emplaced terrestrial lava
356 flows and implications for planetary volcanism, J Geophys Res, 100 (B12), 24509 - 24519,
357 1995.

358 Baloga, S., L.S. Glaze, D. Crisp, and S.A. Stockman, New statistics for estimating the bulk
359 rheology of active lava flows: Puu Oo examples, J Geophys Res, 103, 5133-5142, 1998.

360 Baloga, S.M., L.S. Glaze, M.N. Peitersen, and J.A. Crisp, Influence of volatile loss on thickness
361 and density profiles of active basaltic flow lobes, J Geophys Res, 106 (B7), 13,395 -
362 13,405, 2001.

363 Chandrasekhar, S., Stochastic problems in physics and astronomy, Reviews of Modern Physics,
364 15, 1 – 87, 1943.

365 Crisp, J.A. and S.M. Baloga, A model for lava flows with two thermal components, J Geophys
366 Res, 95, 1255-1270, 1990.

367 Crown, D.A., and S.M. Baloga, Pahoehoe toe dimensions, morphology, and branching
368 relationships at Mauna Ulu, Kilauea Volcano, Hawaii, Bull Volcanol, 61, 288-305, 1999.

369 Danes, Z.F., Dynamics of lava flows, J Geophys Res, 77, 1430-1432, 1972.

370 Glaze, L.S. and S.M. Baloga, 2013, Simulation of inflated pahoehoe lava flows, J Volcanol
371 Geotherm Res, 256, 108-123, doi:10.1016/j.jvolgeores.2013.01.018, 2013.

372 Glaze, L.S., S.M. Baloga, W.B. Garry, S.A. Fagents, and C. Parcheta, A hybrid model for leveed
373 lava flows: Implications for eruption styles on Mars, J Geophys Res, 114, doi:
374 10.1029/2008je003278, 2009.
375 Glaze, L.S., S.M. Baloga, S.A. Fagents, R.Wright, The influence of slope breaks on lava flow
376 surface disruption, J Geophys Res, 119, doi:10.1002/2013JB010696, 2014.
377 Hamilton, C.W., Glaze, L, James, M.R., and S.M. Baloga, Topographic and stochastic influences
378 on pāhoehoe lava lobe emplacement, Bull Volcanol, 75, 756, 2013.
379 Harris, A.J.L. and S.M. Baloga, Lava discharge rates from satellite-measured heat flux,
380 Geophysical Research Letters, 36 (L19302), doi:10.1029/2009GL039717, 2009.
381 Harris, A.J.L., and S.K. Rowland, FLOWGO: A kinematic thermo-rheological model for lava
382 flowing in a channel, Bull Volcanol, 63, 20–44, 2001.
383 Harris, A.J.L., J. Dehn, M.R. James, C. Hamilton, R. Herd, L. Lodato, and A. Steffke, Pahoehoe
384 flow cooling, discharge, and coverage rates from thermal image chronometry, Geophysical
385 Research Letters, 34 (L19303), doi:10.1029/2007GL030791, 2007.
386 Harrison, C.G.A., and C. Rooth, The dynamics of flowing lavas, in Volcanoes and
387 Tectonosphere, edited by H. Aoki and S. Iizuka, pp. 103-113, University of Tokyo, Tokyo,
388 1976.
389 Hon, K., J. Kauahikaua, R. Denlinger, and K. Mackay, Emplacement and inflation of pahoehoe
390 sheet flows: Observations and measur4ments of active lava flows on Kilauea Volcano,
391 Hawaii, Geol Soc Am Bull, 106 (3), 351-370, 1994.
392 Keszthelyi, L., S. Self, and T. Thordarson, Application of recent studies on the emplacement of
393 basaltic lava flows to the Deccan Traps, Memoirs – Geol Soc India, 43, 485-520, 1999.
394 Keszthelyi, L., A.S. McEwen, and T. Thordarson, Terrestrial analogs and thermal models for

395 Martian flood lavas, J Geophys Res, 105 (E6), 15,027-15,049, 2000.
396 Keszthelyi, L., S. Self, and T. Thordarson, Flood lavas on Earth, Io and Mars, J Geol Soc, 163
397 (2), 253-264, 2006.
398 Lipman, P.W. and N.G. Banks, AA flow dynamics, Mauna Loa 1984, USGS Prof Pap, 1350,
399 1527-1565, 1987.
400 Nichols, R.L., Viscosity of Lava, J Geo, 47, 290-302, 1939
401 Peck, D.L., Cooling and vesiculation of Alae lava lake, Hawaii, US Geol Surv Prof Pap 935-B,
402 1-59, 1978.
403 Rowland S.K. and G.P.L. Walker, Pahoehoe and aa in Hawai‘i: volumetric flow rate controls the
404 lava structure, Bull Volcanol, 52, 615–628, 1990.
405 Rowland, S.K., A.J.L. Harris, and H. Garbeil, Effects of Martian conditions on numerically
406 modeled, cooling-limited channelized lava flows, J Geophys Res, 109 (E10010),
407 doi:10.1029/2004JE002288, 2004.
408 Self, S., T. Thordarson, L. Keszthelyi, G.P.L. Walker, K. Hon, M.T. Murphy, P. Long, and S.
409 Finnemore, A new model for the emplacement of Columbia River basalts as large, inflated
410 pahoehoe lava flow fields, Geophysical Research Letters, 23 (19), 2689-2692, 1996.
411 Self, S., L. Keszthelyi, and T. Thordarson, The importance of pahoehoe, Annual Reviews of
412 Earth Planetary Science, 26, 81-110, 1998.
413 Shaw, H.R., and D.A. Swanson, (1970), Eruption and flow rates of flood basalts. In Proceedings
414 2nd Columbia River Basalt Symposium, pp. 271-299, Eastern Washington State College
415 Press, Cheney.
416 Sheskin, D.J., Handbook of Parametric and Nonparametric Statistical Procedures, CRC Press,
417 719 pp., 1997.

418 Thordarson, T., and S. Self, The Roza Member, Columbia River Basalt Group: A gigantic
419 pahoehoe lava flow field formed by endogenous processes? J Geophys Res, 103 (B11),
420 27,411-27,445, 1998.
421 Wright, R. and L.P. Flynn, On the retrieval of lava-flow surface temperatures from infrared
422 satellite data, Geology, 31 (10), 893 – 896, 2003.
423 Wright, R., L. Glaze, and S.M. Baloga, Determining the eruption style and composition of
424 terrestrial lavas using hyperspectral satellite data, Geology, doi:10.1130/G32341.1, 2011.
425

426 Figures and Captions

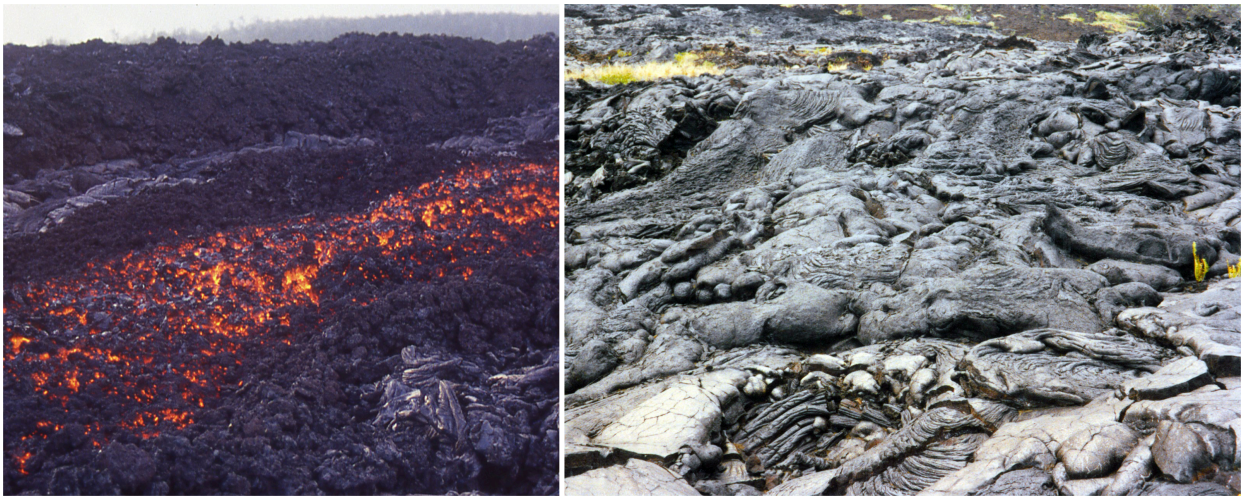

427 (a) (b)

428 Figure 1: (a) Example active channelized a`a lava flow. The key morphologic feature of a`a lava
429 flows is the blocky surface. Indicators of lava transport processes are the raised levees along
430 the lateral flow margins and the central channel containing the flowing lava. Image used
431 with permission of S. Rowland. (b) Field of pahoehoe toes. The key morphologic feature of
432 pahoehoe lava flows is the smooth, often ropy surface. The complexity of pahoehoe transport
433 and emplacement is illustrated by the randomness in dimensions and orientations of the lava
434 toes and lobes in this typical flow field.

435

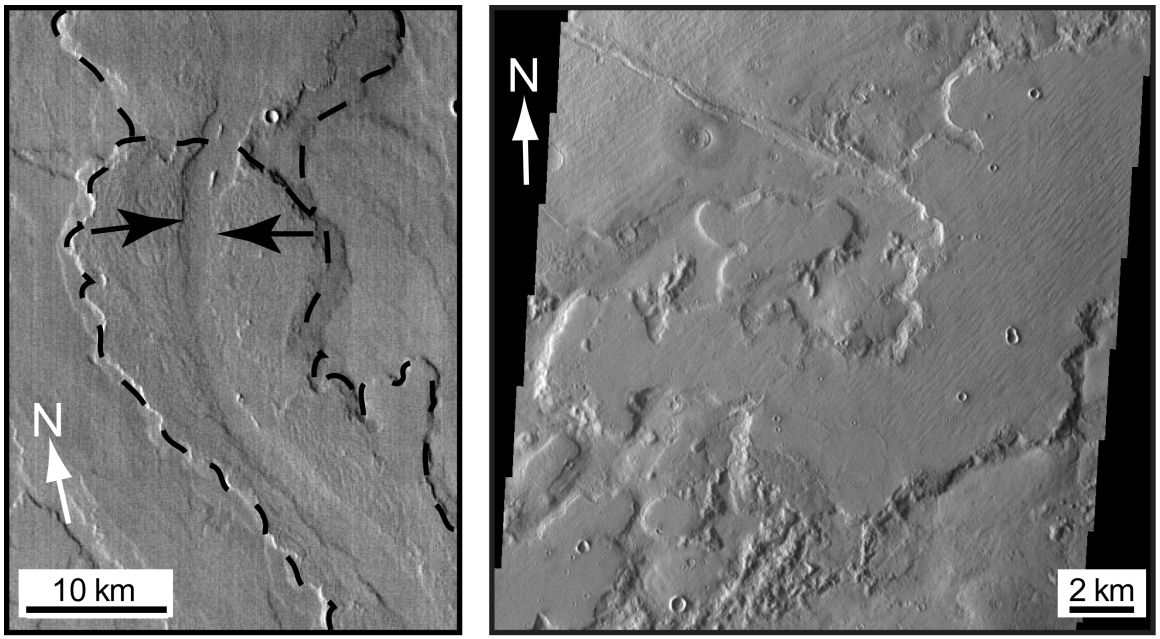


436 (a) N of Pavonis Mons (b) NW of Elysium Mons

437 Figure 2: Examples of (a) a`a channelized flows and (b) putative pahoehoe lava flows on Mars.
438 The a`a flow is characterized by lateral levees (dashed line) and a well-established channel
439 (black arrows) for transporting lava to the flow front. The pahoehoe lava flow is
440 characterized by a broad flat surface that lacks any evidence of a channel, and that is
441 morphologically similar to terrestrial lava flows where pahoehoe lobes have coalesced to
442 form flat plateaus. The flow also exhibits margins with a great deal of variability analogous
443 to terrestrial flows that advance through pahoehoe toe lobes. Figure (a) is a Thermal
444 Emission Imaging Spectrometer (THEMIS) infrared image (frame I01739006). Figure (b) is
445 a THEMIS visible image (frame V14162005).

446

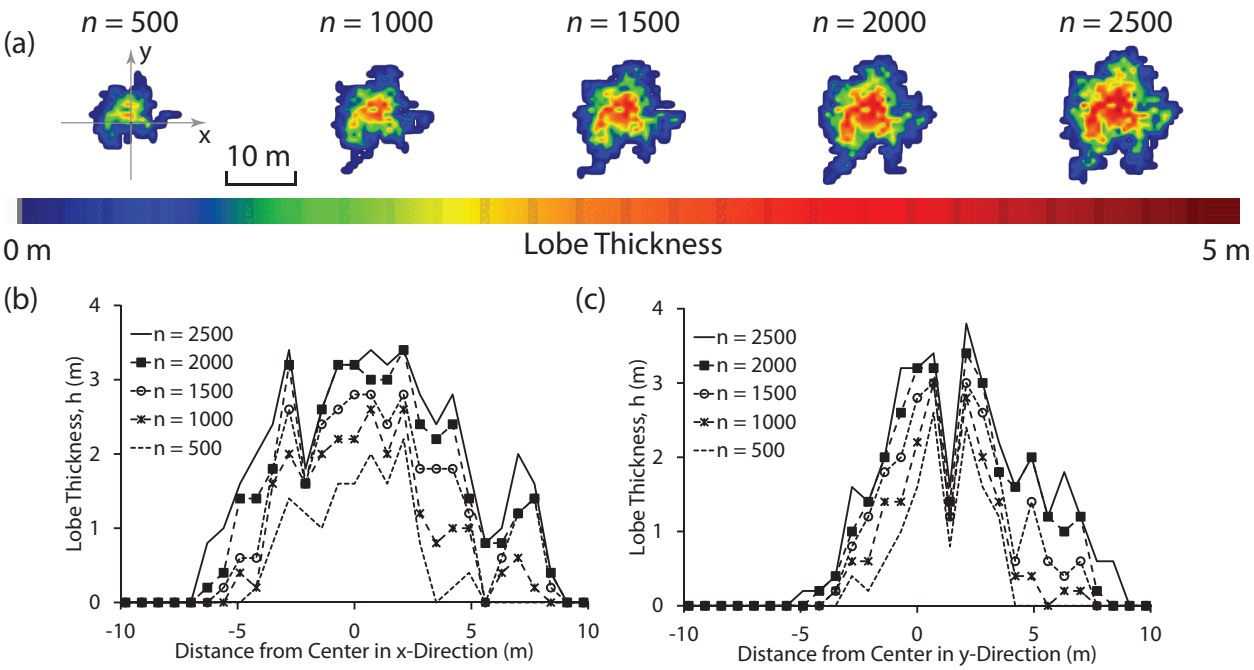


447

448 Figure 3: Typical example of an equiprobable simulation. (a) 3-dimensional topography at five
449 time steps (n = 500, n = 1000, n = 1500, n = 2000, n = 2500). The source parcel location is
450 located at the intersection of the *x* and *y* axes. Corresponding cross-lobe topographic profiles
451 in the (b) *x* and (c) *y* directions are also shown. Generally the lobes are symmetric with the
452 variability in both plan form and topography being typical of field observations. Figure
453 reproduced with permission from *Glaze and Baloga* [2013].

454

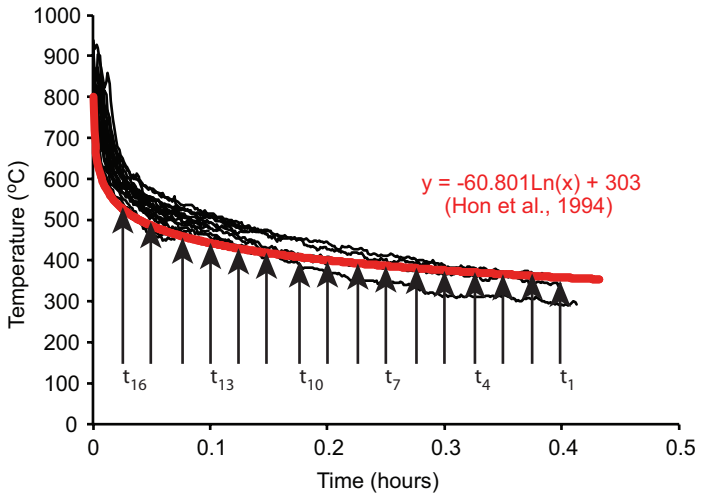


455

456 Figure 4: Pahoehoe surface cooling curves (black) adapted from *Harris and Baloga* [2009] and
457 empirical model (red) from *Hon et al*. [1994]. Model surface temperatures are indicated for
458 16 time steps (where each time step is 90 seconds and every parcel is exposed at the surface
459 for illustration purposes). The first parcel (time step 1) has been exposed at the surface for
460 0.4 hours (1440 s) and has the coolest surface temperature. The most recent parcel (time step
461 16) has only been exposed for 90 seconds and has the highest surface temperature.

462

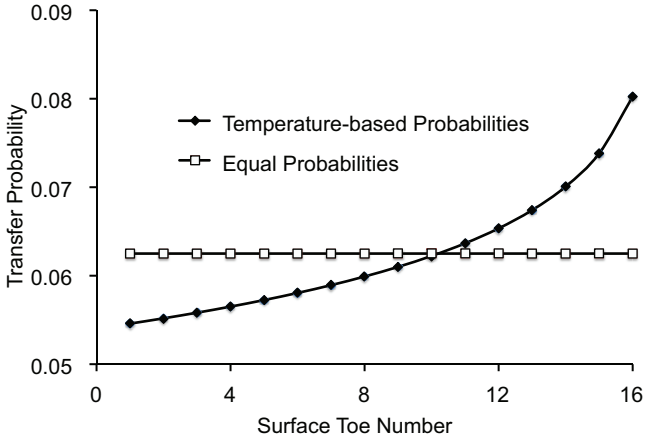


463

464 Figure 5: Transfer probabilities for the temperature dependent model (solid diamonds)
465 corresponding to the time steps shown in Figure 4. Probabilities are directly correlated to the
466 surface temperature and the length of time a parcel has been exposed at the surface (all
467 parcels are exposed at the surface for this example). Toe 16 is the most recent parcel to be
468 exposed. Thus it has the highest surface temperature and the highest likelihood to be the
469 location of the subsequent parcel transfer. The equiprobable distribution is shown with open
470 squares for comparison.

471

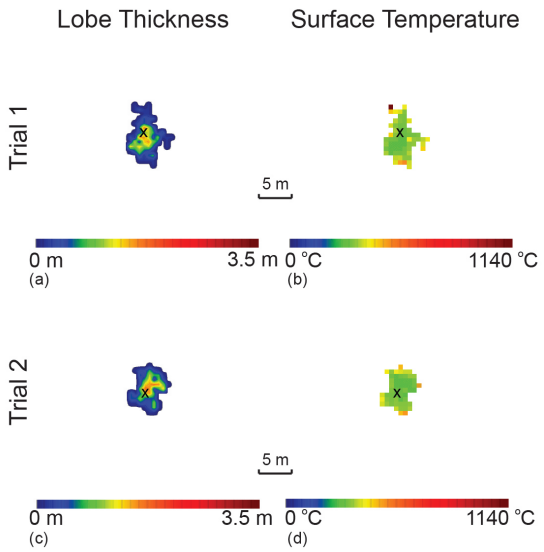


Figure 6: Two example temperature-dependent simulations (Trials 1 and 2) with 200 parcels each. The location of the initial parcel is indicated by an 'x'. In each Trial, the left panel shows a smoothed representation of the lobe thickness, and the right panel shows the surface temperature.

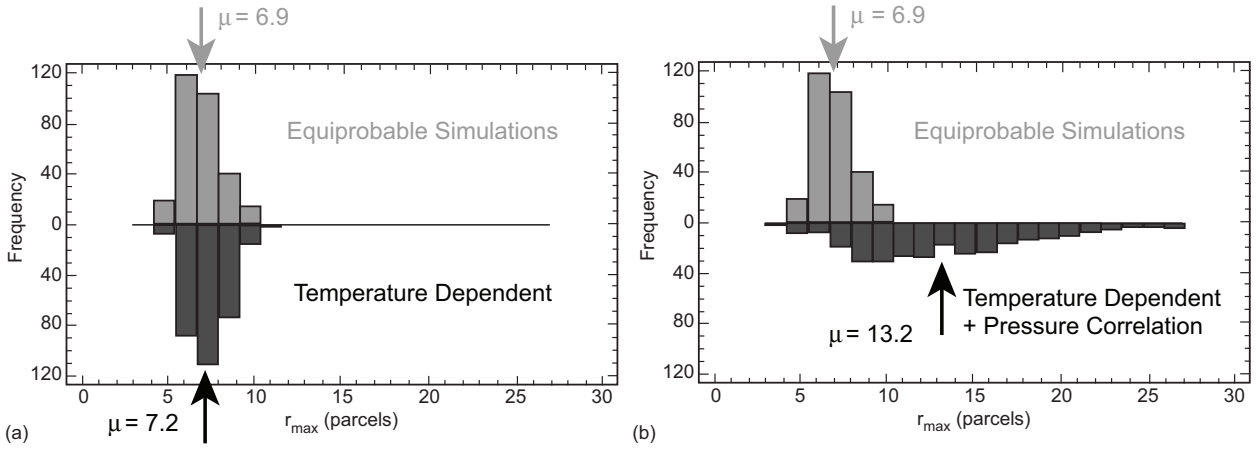


Figure 7: Distribution of maximum distance traveled ($r_{max}$) in 300 simulations. (a) Comparison of $r_{max}$ for 300 equiprobable simulations with 300 temperature-dependent simulations. (b) Comparison of 300 equiprobable simulations to 300 simulations with both temperature dependent probabilities and correlations based on increased pressure following internal transfers.

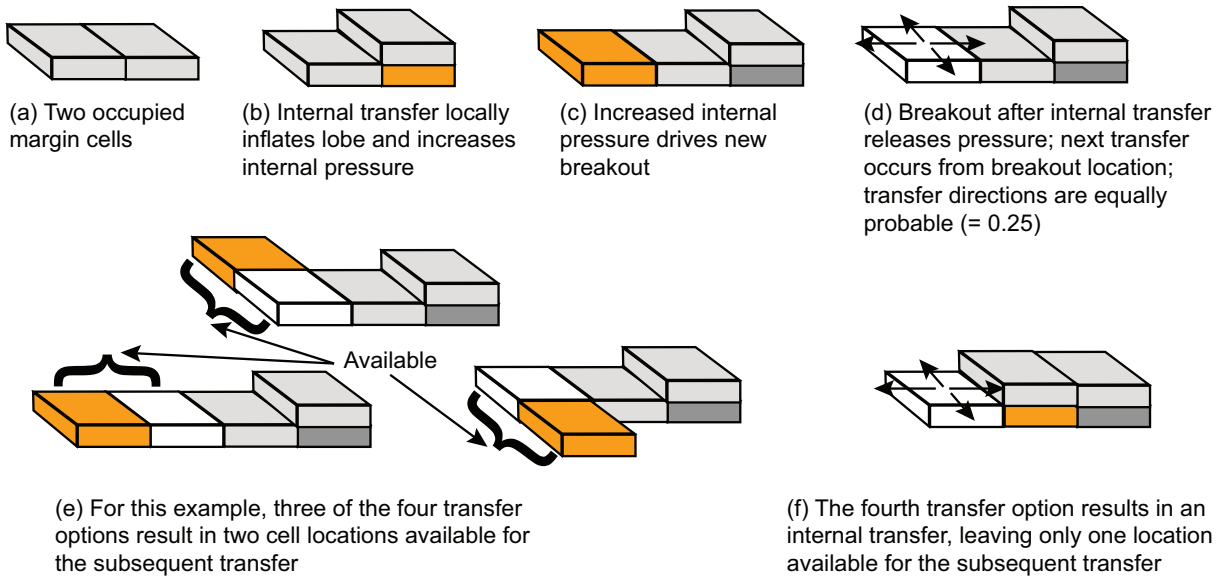


485

486 Figure 8: Cartoon illustrating the influence of pressure buildup at the location of two occupied
487 cells along the lobe margin (a) following inflation due to one or more internal parcel transfers
488 (b). Following a new breakout expanding the lobe's areal extent (c), only the most recently
489 occupied locations (weakest crust) are available for future parcel transfers (d – f). The net
490 result of the pressure effect is to elongate the planform shape of the lobe.

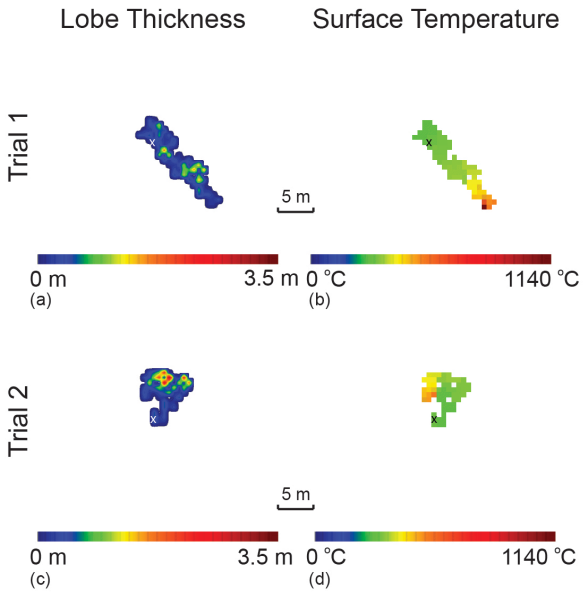


491

492 Figure 9: Two example simulations (Trials 1 and 2) with 200 parcels each with both
493 temperature-dependent probabilities and pressure correlation. The location of the initial
494 parcel is indicated by an 'x'. In each Trial, the left panel shows a smoothed representation of
495 the lobe thickness, and the right panel shows the surface temperature.

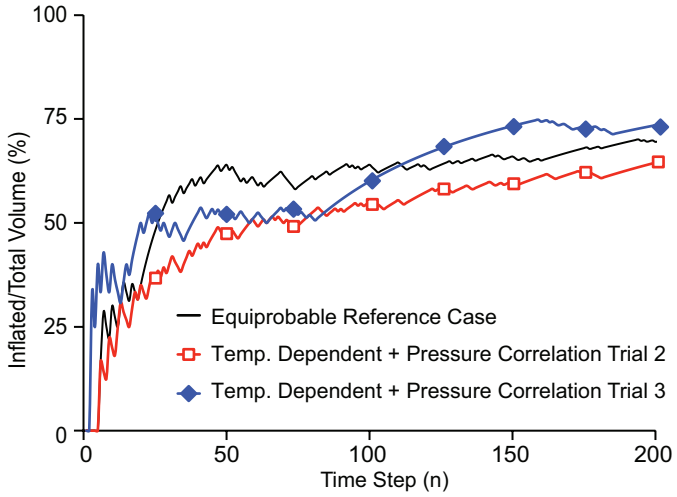


496

497 Figure 10: Three example simulations with 200 parcels each. The fraction of the total lobe
498 volume that is represented by internal parcel transfers (transfers that increase the lobe volume
499 without increasing the lobe area) is shown for the Equiprobable reference case as well as two
500 independent trials of the pressure-dominated case.